TRIBOLOGIA - Finnish Journal of Tribology 1-2 vol 39/2022

https://doi.org/10.30678/fjt.107475

SUOMEN TRIBOLOGIAYHDISTYS RY
THE FINNISH SOCIETY FOR TRIBOLOGY
www.tribologysociety.fi
https://journal.fi/tribologia

Tribological Performance of the Continuous Steel Fiber-reinforced Cu based Friction Material for Heavy-duty Braking Applications

Dr. R. Vaira Vignesh, V. Sai Pranay, Pavan Kalyan Kota, Dr. M. Govindaraju

Department of Mechanical Engineering, Amrita School of Engineering, Coimbatore, Amrita Vishwa Vidyapeetham, India.

Corresponding author: Dr. R. Vaira Vignesh (r_vairavignesh@cb.amrita.edu)

ABSTRACT

Brake pads are the major components of the wind turbine, which primarily consists of metal matrix and ceramic reinforcements. The ceramic particles plunge out during the application of brakes, which in turn leads to the transformation of the wear mechanism from adhesive to abrasive wear. This increases the wear rate and therefore the study investigates the possible replacement of ceramic reinforcements with continuous fibers that exhibit high strength and compatibility. In recent years, Cu-based brake pads that are fabricated by powder metallurgy route are widely used in wind turbines. In this study, continuous fibers of stainless steel SS304 are reinforced in the Cu matrix by the casting method to preserve the fiber alignment. The fabricated composite is characterized for microstructure, microhardness, and tribological behavior. Besides, a comprehensive analysis of the wear mechanism in the developed composite is presented based on the surface morphology, elemental composition, and phase analysis.

Keywords: Ceramic reinforcements, continuous fiber, casting, copper, SS304

1. INTRODUCTION

Over the years, the uninterrupted extraction and usage have caused the depletion of fossil fuels. Besides the limited availability, the greenhouse effect caused by the emission of burning fossil fuels haunts the world [1]. Novel methods are being investigated to counteract this problem, and one of them is through the use of renewable energy sources (green energy). The term green energy predominantly refers to the energy obtained from the sun, wind, tides, thermal and hydro resources of the earth. Among the other renewable energy sources, the chief source of energy is wind energy [2, 3]. With the help of wind turbines, the kinetic energy of wind is converted into electrical energy.

The wind characteristics are not the same always and some unforeseeable wind patterns are a major threat to the wind turbine. Therefore, the economic and safe operation of the wind turbines is reliant on the braking system. Hence, the braking system is regarded as a crucial part of the wind turbine [4]. The conventional braking systems in the wind turbines are:

- Primary Braking system (Aerodynamic)
- Secondary Braking System (Mechanical)

In the aerodynamic braking system, the rotor blades are positioned perpendicular to the airflow to convert kinetic energy into mechanical energy. This rotor blade position is called the aerodynamic braking position. The mechanical brakes are disk brakes that are routinely used during maintenance, repair work, or emergencies when the wind speed is quite high [5]. The brakes should have excellent heat dissipation, high wear resistance, and be long-lasting [6, 7]. The conventional brake pads tend to wear pretty early and therefore need to be changed frequently [8-10]. Research in this area is thus needed to make the brakepads more durable and more resistant to wear.

Cu is the most commonly used material in brake pads because of its good brake performance characteristics and excellent thermal conductivity [11-14]. Besides, Cu enables a stable friction coefficient and stabilizes smooth sliding [15 -17]. Habin Zhou et al., [18] studied the wear behavior and friction characteristics of Cu matrix composite with varying percentages of Fe. Composites containing 10-15% of Fe exhibited a lower coefficient of friction (COF) and wear rates. Adhesion wear mechanism dominated the composites with low (<5 vol.%) Fe content. Oxidation and delamination was the main wear mechanism for (5 vol.% to 15 vol.%) moderate iron content. Delamination was the main wear mechanism for high (> 15 vol.%) iron content.

Peng Zhang et al., [19] studied the influence of the composition of Fe powder on the tribological characteristics of Cu matrix composites. The composite specimen with 30.6% Fe had the highest wear rate. The wear loss of the brake pad was found out to be 0.25 cm^3/MJ, which is 29% lower than that of the specified limit i.e. 0.35 cm^3/MJ. However, the composite exhibited the most stable friction coefficient among the tested specimens. Peng Zhang et al.,

[20] studied the fade behavior of a Cu-based brake pad under emergency braking conditions (high speed and overload). The results indicated that the formation of fatigue cracks and an increase in temperature led to the softening of the Cu-rich surface. The rapid transfer of the friction layer weakened the brake pad that caused a severe fading effect.

Gultekin et al., [21] investigated the frictional and wear characteristics of graphite-reinforced Cu matrix composite brake pad against Al-SiCp composite. The COF of the composite varied between 0.2 and 0.45, and the COF decreased with an increase in load, due to the presence of graphite. The formation of a friction layer on the worn-out surface confirmed the presence of carbon and copper oxides. The Al-SiCp composite exhibited lower wear, which was attributed to the presence of SiC particles.

Said Abdi et al., [22] explored the mechanical and tribological properties of Cu composite with stainless steel reinforcements. The reinforcement of stainless steel resulted in higher hardness, which in turn increased the wear resistance of the composite. The heat treatments of the composite increased the tensile strength. Peng Zhang et al., [23] studied the effect of the use of Al_2O_3 fibers in Cu-based brake pads. The addition of Al_2O_3 contributed to an increase in the COF in low sliding speed and low-pressure conditions. However, the Al_2O_3 fibers stabilized the COF at high sliding speed and pressure. Suckhoon Kang et al., [24] studied the friction and wear characteristics of Cu-based and Fe-based friction material in brake pads. At low load, Cu-based specimens shown excellent tribological properties. However, the Cu-based specimen displayed a fading effect. Interestingly, the Fe-based specimen exhibited a lower wear rate and stabilized COF at high loads.

Hamada et al., [25] studied the hot deformation behavior of stainless steel fiber-reinforced Cu matrix composite between 700°C and 1000°C. The metallographic observations revealed that the dynamic recrystallization resulted in ultrafine-grained structures in the stainless steel fibers. Besides, the stainless steel fibers increased the strength of the composite at lower temperatures. Osterle et al., [26] studied the effect of Cu in brake pads and brake performance properties. The Cu chips used on the surface of the pad showed zones of high plastic deformation, which in turn provided high hardness. Cu acts as a solid lubricant when it is detached from the surface and included in friction layers. Further analysis showed that the use of Cu leads to stabilization in smooth sliding and frictional force. The brief review of the literature highlights that fiber reinforced friction material for heavy-duty applications is in the developmental stage. Hence, continuous steel fiber reinforced copper-based friction materials are seldom discussed in the open literature. This study focus on the development of continuous fiber reinforced brake pad materials.

In this study, continuous stainless steel fibers were reinforced in the Cu matrix by the casting technique. The fabricated composites were characterized by microstructural, mechanical, and tribological properties. The study presents the predominant wear mechanism of the developed composite at various loads, which was determined using analytical instruments.

2. Materials and methods

2.1 Materials

In this study, commercially available Cu rods (99.99% purity) and stainless steel SS304 fibers (0.2 mm) were utilized. The composition of SS304 fibers is given in Table 1.

Element	Composition (Weight %)
Carbon, C	0.06 %
Chromium, Cr	19.26 %
Iron, Fe	68.67%
Manganese, Mn	1.75 %
Nickel, Ni	9.47%
Phosphorous, P	0.03 %
Silicon, Si	0.74 %
Sulfur, S	0.02 %

Table 1. SS-304 Composition

2.2 Fabrication

Mild steel was used to fabricate a cylindrical die of inner diameter 25 mm and length 50 mm. The SS304 fibers were positioned parallelly to the axis of the cylindrical die. The die-setup was preheated to 250°C to avoid casting defects. The Cu rods were molten in an alumina crucible using an induction furnace and poured into the preheated die-setup. The composition of the metal matrix composite (MMC) is given in Table 2.

Material	Composition (wt.%)
Copper	98%
SS-304 fibers	2%

Table 2. Material composition

2.3 Microstructure and Microhardness

The cast specimens were prepared and were polished as per the standard ASTM E3-11. The samples were disc polished using 400 grit, 800 grit, 1000 grit, and 1200 grit metallographic sheets until a mirror finished was obtained. The polished specimens were etched and the microstructures were observed using an optical microscope (Carl Zeiss, Axiovert 25) at various magnifications. The Vickers microhardness of the cast specimens was tested using a microhardness tester (UHL, VMHT 104) at a load of 300 gf that acted for a dwell time of

15 s. The average microhardness of five indentations was reported.

2.4 Tribological test

Specimens of diameter 25 mm and length 25 mm were used to study the tribological characteristics in a pin-on-disc tribometer (Ducom, TR20LE). The test specimens were prepared by mounting a hollow steel tube using the cold setting compound. The specimens were slid at a sliding velocity of 6.28 m/s for 10 minutes under the action of axial loads (1 kg, 2 kg, 3 kg, 4 kg, and 5 kg) against the counter disc made of EN31 steel (with an average hardess of 63 HRC). The average tribological result (wear rate and coefficient of friction) of three specimens is reported. The specimens were weighed using a precision weighing balance with a readability of 0.0001 g before and after the tribological test to calculate the mass loss. The wear rate was determined using the equation (1).

$$Wear\ rate = \frac{Mass\ loss\ (g)}{Axial\ load\ (N) \times Sliding\ Distance\ (m)} \quad (1)$$

2.5 Surface Morphology and X-Ray Diffraction analysis

The surface morphology of the worn specimens was obtained by using a high-resolution scanning electron microscope (Zeiss Sigma, Gemini), under various ranges of magnification and suitable electron acceleration voltage. The elemental composition and elemental distribution were obtained using an energy dispersive X-ray spectroscope (Oxford Instruments). The phase composition was analyzed using an X-ray diffractometer (Rigaku, Ultima 4) using Cu-Kα radiation in continuous scanning mode at a scan rate of 0.5°/minute between 10° and 90°.

3. Results and Discussions

3.1 Microstructure and Microhardness

Figure 1 shows the embedment of SS304 fibers in the Cu matrix of the developed composite specimen. Besides,

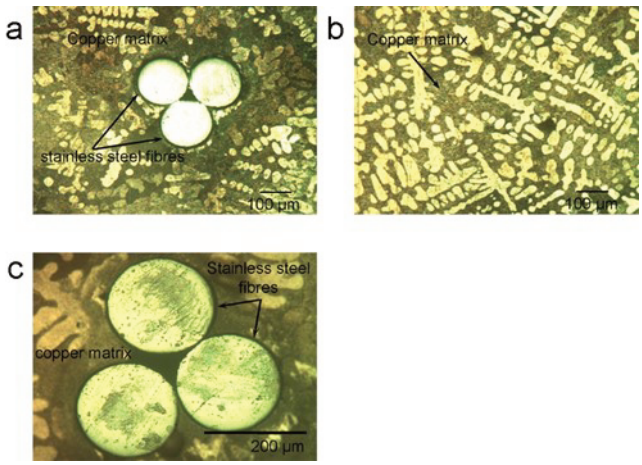

Fig. 1. Microstructure of the developed composite that shows (a) Copper matrix and SS304 fibers; (b) Copper matrix; (c) Magnified view of the SS304 fibers

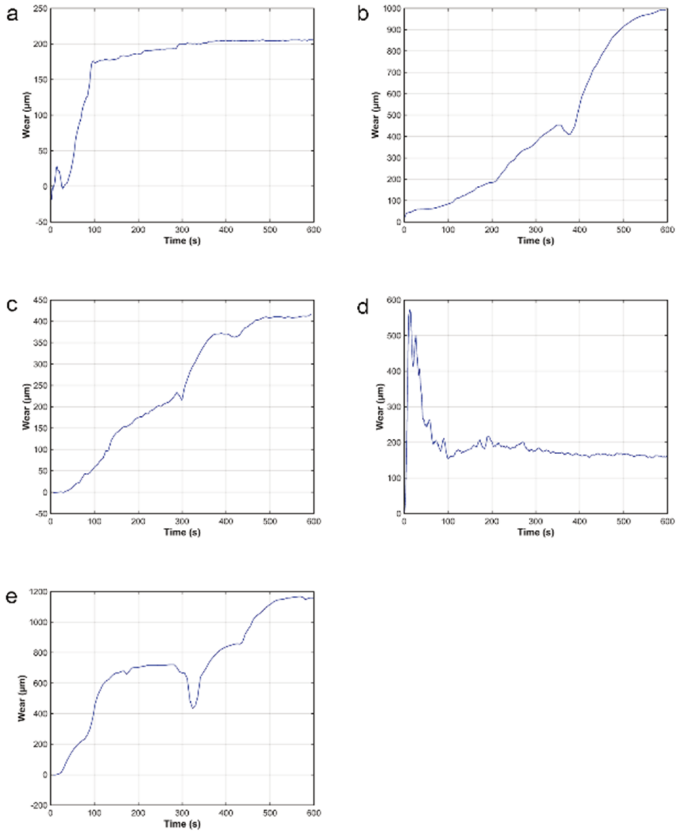

Fig. 2. Wear of the composite specimen with increase in sliding time at normal load of (a) 1 kg; (b) 2 kg; (c) 3 kg; (d) 4 kg; (e) 5 kg

the microstructure analysis confirmed that the orientation of the SS304 fibers remained the same after the casting process. Also, the absence of porosity and micro-defects established good bonding between the Cu and SS304 fibers. The microhardness of the Cu matrix and SS304 fibers were found to be 68±2.3 HV0.3 and 163±3.1 HV0.3 respectively, which is consistent with the available literature [15, 16, 27-29].

3.2 Tribological Performance

Wear of the composite specimen with an increase in the sliding time. The wear test was performed on a pin-on-disc tribometer with a sliding velocity of 6.28 m/s for 10 minutes under various load conditions (1 kg, 2 kg, 3 kg, 4 kg, 5 kg). Figure 2 illustrates the wear (in µm) of the developed composite with time. Figure 2 (a) shows the wearing trend of the composite specimen that was worn at a load of 1 kg. The graph shows a gradual increase in wear of the composite, which was followed by stable wear after 300 s. Figure 2 (b) shows the wear of the composite specimen with time at a load of 2 kg. The specimens exhibited a gradual increase in wear with an increase in time, which was followed by an exponential increase in wear. With an increase in load, the breakage of asperities and the formation of wear debris increased the wear of the composite specimen after 400 s. A similar trend was observed in the composite specimen worn at a load of 3 kg

and 5 kg, as observed in Figure 2 (c) and Figure 2(e). However, the composite specimen worn at 4 kg load exhibited high wear initially which was followed by a reduced and stabilized wear after 100 s, as evident from Figure 2(d). Detailed analysis of the wear mechanism and the formation of oxide layers is presented in the following sections.

3.3 Wear rate of the composite specimen

The wear rate of the composite specimen at various loads is shown in Figure 3 that shows a decrease in the wear rate of the composite specimen with an increase in the load. Specimen subjected to 1 kg load had the highest wear rate of 1.0036×10^{-6} g/Nm while the specimen subjected to 3 kg load had the least wear rate of 1.3831×10^{-7} g/Nm. The wear rate of the specimen was lesser than the conventional brake pads at all loading conditions [8, 17].

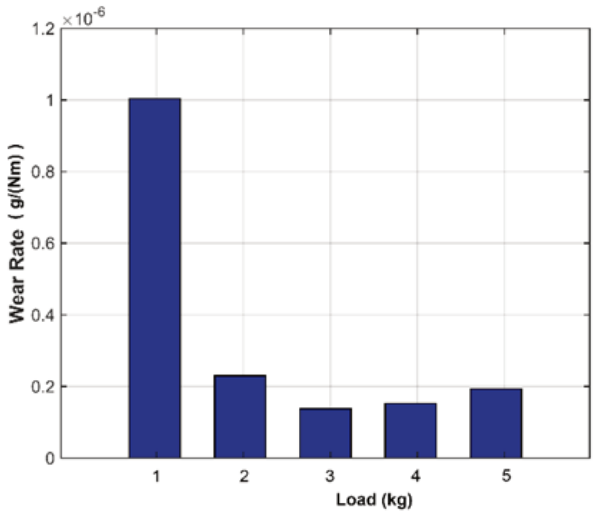

Fig. 3. Wear rate of the composite specimen at various normal loads

Normal load of 1 kg

The wear mode of the worn composite specimens at all loads with a comprehensive analysis of the elemental composition, elemental distribution, and phases in the composite specimen that exhibited the highest and the least wear rate are described in the following section. The surface morphology of the specimen worn under a normal load of 1 kg is shown in Figure 4. Delamination, grooves, and micro-cracks were observed in the worn composite specimen, as shown in Figure 4 (a). Figure 4 (b) shows the SS304 fibers along with the striations produced by the wear test. As observed in Figure 4 (c), the worn composite specimen had delamination, wear debris, and protrusions on the surface. The surface morphology analysis indicates a combined adhesive and abrasive wear phenomenon in the composite specimen.

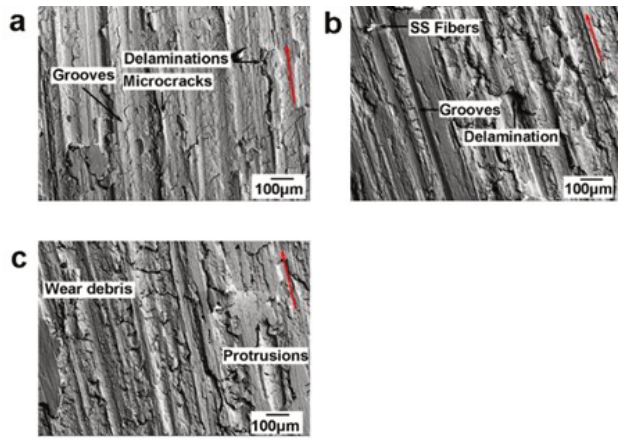

Fig. 4. Surface morphology of the composite specimen worn at a normal load of 1 kg

Figure 5 represents the elemental composition of the worn composite specimen with major counts for Cu (matrix) followed by Fe (SS304 reinforcement or embedded Fe particles from the counter disc) and minor counts for O. This indicated the absence of oxidation phenomenon in the worn composite specimen.

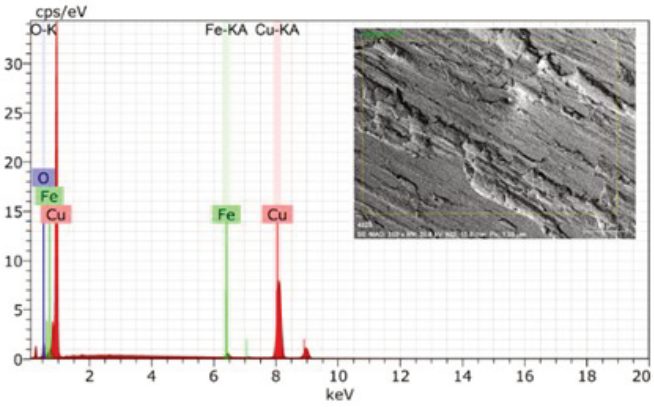

Fig. 5. Elemental composition of the composite specimen worn at a normal load of 1 kg

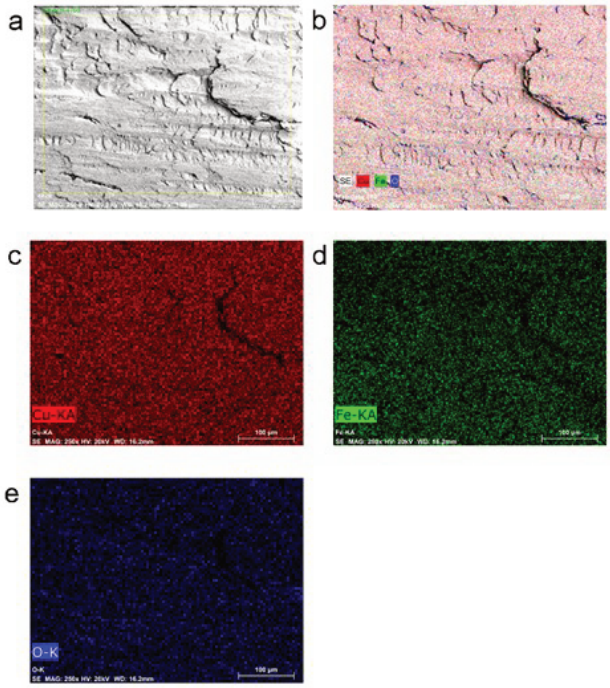

Fig. 6. Elemental distribution in the composite specimen worn at 1 kg normal load (a) Chosen area; (b) Consolidated elemental map; (c) Distribution of Cu; (d) Distribution of Fe; (c) Distribution of O

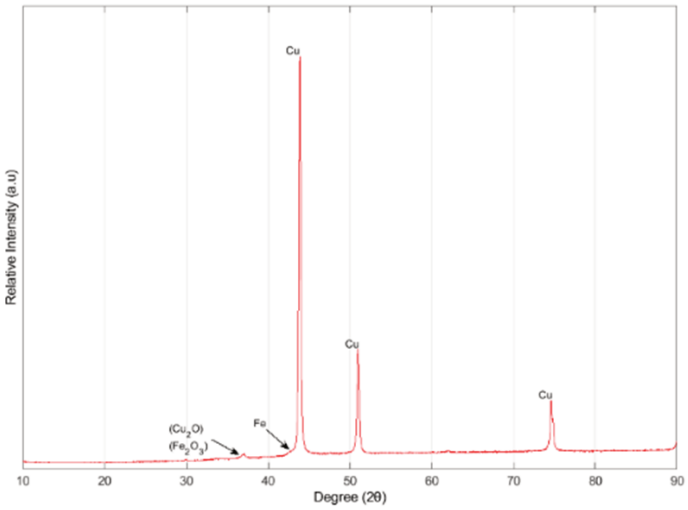

Fig. 7. Compositional phases in the composite specimen worn at1 kg normal load

Further, elemental mapping was performed to analyze the distribution of elements in the worn composite specimen. Figure 6 (a) shows the chosen area for elemental mapping and Figure 6 (b) shows the consolidated elemental map of the worn composite specimen. In line with the elemental composition results, the distribution of Cu was higher in the matrix (Figure 6 (c)), which was followed by Fe (Figure 6 (d)). The distribution and concentration of O were meager in the worn composite specimen, as evident from Figure 6 (e).

Besides, XRD analysis also indicates significant peaks for Cu and Fe and less intense peaks for oxides of Cu and Fe. The results indicate a meager possibility for surface oxidation, which is attributed to the high wear rate of the composite specimen worn at 1 kg load as shown in Figure 7.

Normal load of 2 kg

The surface morphology of the specimen worn at a normal load of 2 kg is shown in Figure 8. Figure 8 (a) shows the voids, protrusions, and delamination, which were formed by the cyclic impact of abrasive particles at

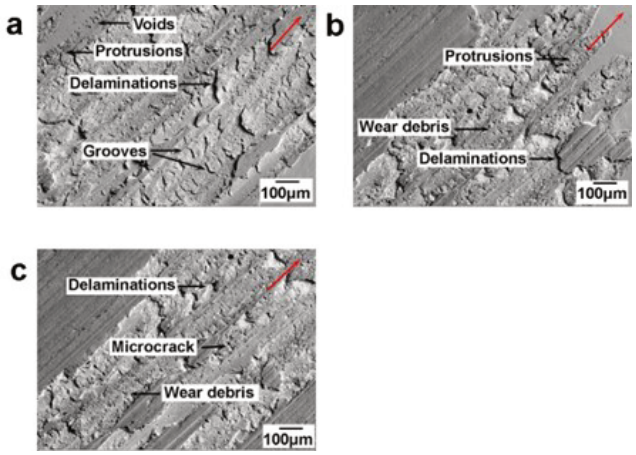

Fig. 8. Surface morphology of the composite specimen worn at a normal load of 2 kg

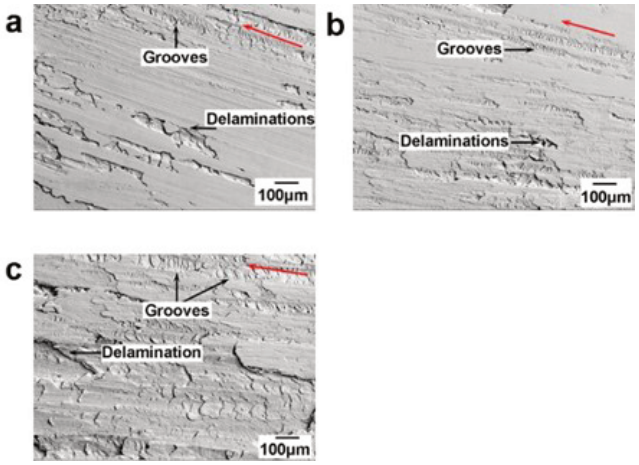

Fig. 9. Surface morphology of the composite specimen worn at a normal load of 3 kg

the interface. Figure 8 (b) shows the formation of protrusions and more quantity of wear debris on the worn surface. Besides, deep grooves and micro-cracks were observed on the worn surface of the composite specimen (Figure 8 (c)). It is therefore concluded that the predominant wear mechanism in the composite specimen worn at 2 kg load is a combination of adhesive and abrasive wear.

Normal load of 3 kg

The surface morphology of the specimen worn under a normal load of 3 kg is shown in Figure 9. Delamination and grooves were observed in the worn composite specimen, as shown in Figure 9 (a) to Figure 9 (c). The surface morphology analysis indicated an adhesive wear phenomenon in the composite specimen.

The elemental composition of the worn composite specimen that is shown in Figure 10 indicates major counts for Cu followed by Fe. The counts for O in the composites specimen worn at 3 kg load was slightly higher than that of the composite specimen worn at 1 kg. This indicated the

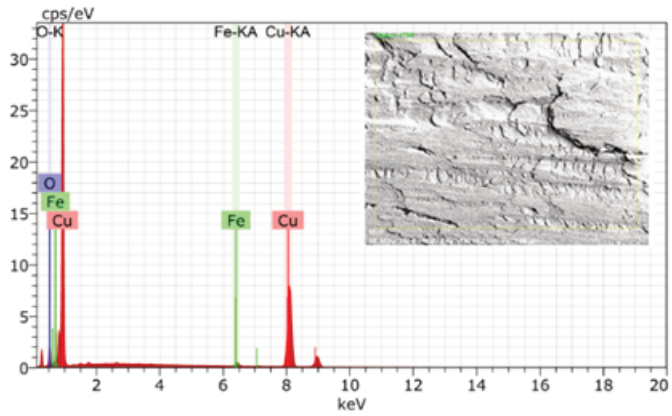

Fig. 10. Elemental composition of the composite specimen worn at a normal load of 3 kg

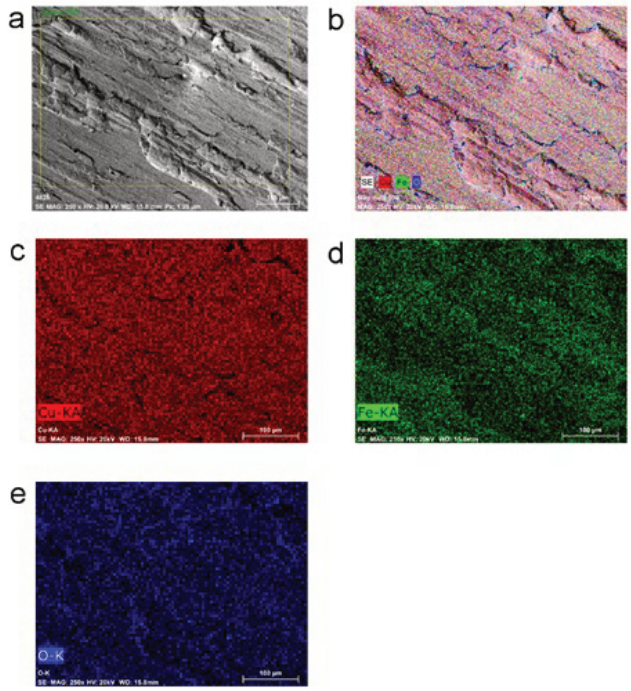

Fig. 11. Elemental distribution in the composite specimen worn at 3 kg normal load (a) Chosen area; (b) Consolidated elemental map; (c) Distribution of Cu; (d) Distribution of Fe; (c) Distribution of O

surface oxidation phenomenon in the worn composite specimen.

Furthermore, elemental mapping of the worn composite specimen is shown in Figure 11. Figure 11 (a) shows the chosen area for elemental mapping and Figure 11 (b) shows the consolidated elemental map of the worn composite specimen. In line with the elemental composition results, the distribution of Cu was higher in the matrix (Figure 11 (c)), which was followed by Fe (Figure 11 (d)). The distribution and concentration of O were comparatively high in the worn composite specimen, as evident from Figure 11 (e).

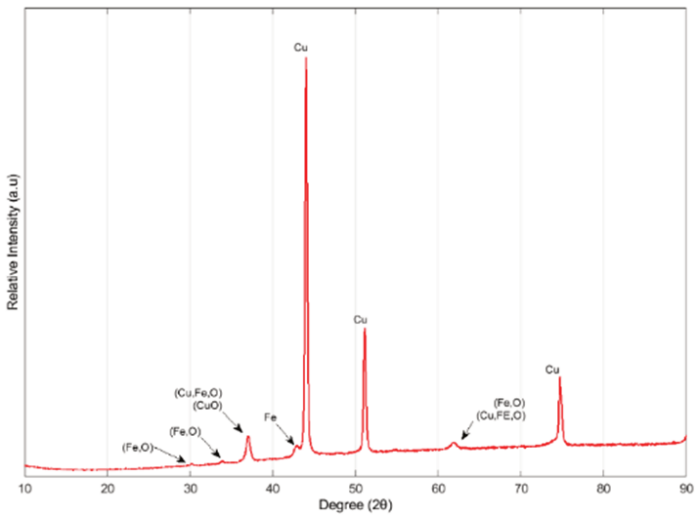

Fig. 12. Compositional phases in the composite specimen worn at 3 kg normal load

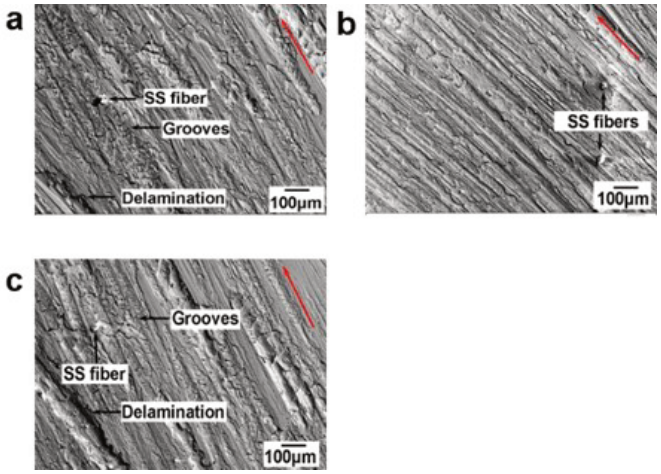

Fig. 13. Surface morphology of the composite specimen worn at a normal load of 4 kg

In addition, XRD analysis also indicates significant peaks for Cu, Fe, oxides of Cu, and Fe, as shown in Figure 12. The results indicate a surface oxidation phenomenon, which reduces the wear rate of the composite specimen worn at a 3 kg load to 1.3831×10^{-7} g/Nm.

Normal load of 4 kg

Figure 13 shows the surface morphology of the composite specimen worn at a normal load of 4 kg. Figure 13 (a) shows the SS304 fiber (partial) with heavy deformation and striations. The protrusions and deep grooves were observed in the worn region, as shown in Figure 13 (b). Figure 13 (c) spots the delaminated regions and voids in the worn composite specimen. From the worn surface morphology analysis, it is perceived that the wear transits from mild to severe region. This transition increased the wear rate of the composite specimen to 1.5285×10^{-7} g/Nm with an increase in load from 3 kg to 4 kg.

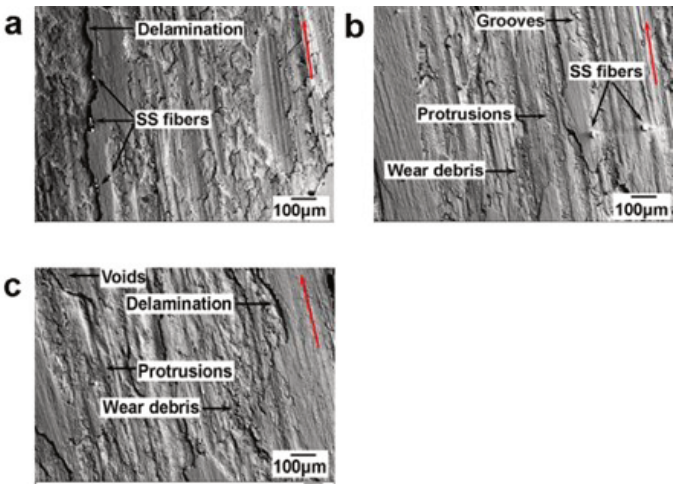

Fig. 14. Surface morphology of the composite specimen worn at a normal load of 5 kg

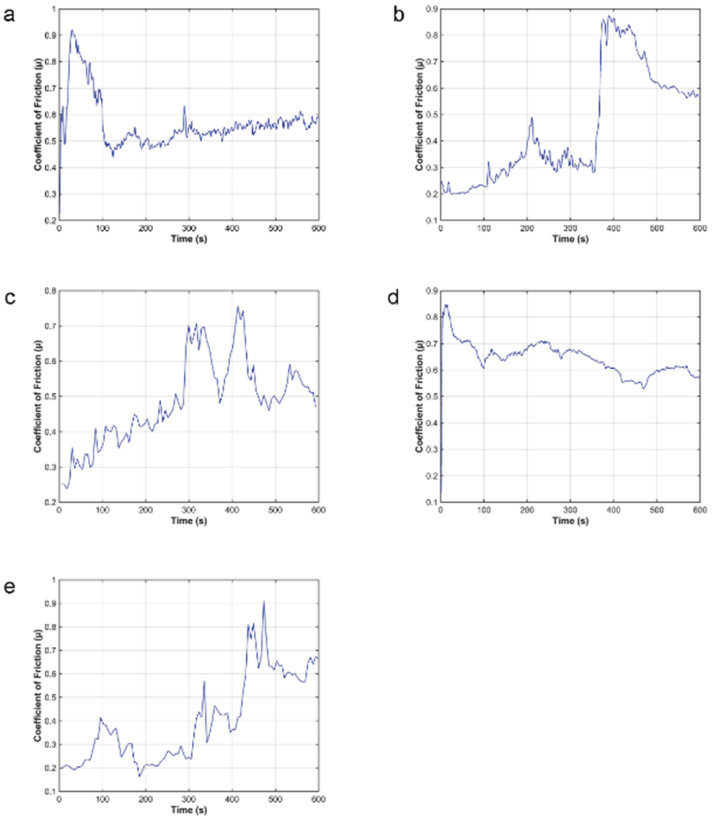

Fig. 15. COF of the composite specimen with increase in sliding time at normal load of (a) 1 kg; (b) 2 kg; (c) 3 kg; (d) 4 kg; (e) 5 kg

Normal load of 5 kg

Figure 14 shows the worn surface morphology of the composite specimen that was worn at a normal load of 5 kg. Figure 14 (a) shows a portion of SS304 fiber with delamination and ridges along the sliding direction. Figure 14 (b) shows the shallow grooves and scratch marks on the worn surface. Besides, Figure 14 (c) shows grooves and small delamination on the worn surface of the composite specimen.

It is therefore concluded that the predominant wear mechanism in the composite specimen worn at 5 kg load is a combination of adhesive and abrasive wear. Hence, the wear rate of the composite worn at 5 kg was ~1.26 times higher than that of the composite specimen worn at 4 kg.

3.4 Coefficient of friction of the composite specimen with an increase in the sliding time

Figure 15 illustrates the typical COF of the developed composite concerning time. Figure 15 (a) displays the COF trend of a specimen worn at a load of 1 kg. The graph shows an increase in the COF in the initial stages and then stabilizes in a range of 0.5 to 0.6 after 300 s. Figure 15 (b) shows the COF of the composite specimen worn at a 2 kg load. The COF was observed to gradually increase with time. However, a sudden increase in the COF (0.85) was noticed at 370 s, which eventually decreased. This is attributed to the adhering / influence of wear debris particles at the contact interface.

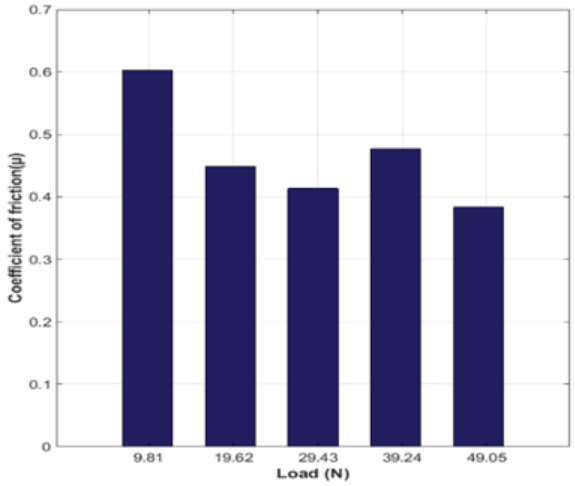

Fig. 16. COF of the composite specimen at various normal loads

Figure 15 (c) shows an erratic behavior where the friction coefficient increased continuously and exhibited a sudden rise at 450 s. This is also attributed to the influence of wear debris particles at the contact surface. Similar behavior was observed in the composite specimen worn at a normal load of 5 kg, as shown in Figure 15 (e). The composite worn at 4 kg load exhibited a high COF of 0.85 as evident from Figure 15 (d). The COF fluctuated between 0.50 and 0.70 in the composite specimen.

3.5 Coefficient of friction at various normal load

The average COF at the various normal loads is shown in Figure 16. From the graph, it is observed that the average COF decreased with an increase in normal load. Among the tested composite specimens, the composite specimen worn at a normal load of 1 kg exhibited the highest average COF (0.60), whereas the composite specimen worn at a normal load of 5 kg sample exhibited the least average COF (0.38).

4. Conclusion

The Cu-based metal matrix composite with SS304 fibers as reinforcement was fabricated successfully by casting technique for brake pad application. The microstructure, microhardness, and tribological characteristics of the fabricated composite were analyzed. The results demonstrated the following:

1. The microstructure analysis revealed that the SS304 fibers remained oriented along the central axis of the composite. Besides, good bonding was observed between the Cu matrix and SS304 fibers. The reinforcements were uniformly distributed, and no micro defects or porosity were observed.
2. The microhardness of the Cu matrix and SS304 fibers were found to be 68±2.3 HV0.3 and 163±3.1 HV0.3, which are consistent with the available literature.
3. The wear test showed that the specimen worn at a normal load of 3kg exhibited the least wear rate of 1.3831×10^{-7}g/Nm. The delamination and formation of

oxide layers were considered to be the dominant wear mechanisms in the developed composite. The COF was found to vary between 0.4 to 0.6.

4. The reinforcement of SS304 fibers comparatively resulted in higher wear resistance than the conventional brake pad friction material.

ACKNOWLEDGEMENT

The authors are thankful to the Department of Science and Technology and Quantum Heat Treaters Pvt. Ltd., for their financial support to carry out this investigation through a research project titled "Development, Field Trials, Pilot Production, and Technology Demonstration of Sintered Braked Pads with Improved Performance for Wind Turbine Applications Suitable to India Specific Wind Characteristics" (DST/TDT/AMT/2017/002(G)).

REFERENCES

[1] Kweku, D. W., Bismark, O., Maxwell, A., Desmond, K. A., Danso, K. B., Oti-Mensah, E. A., Quachie, A. T., and Adormaa, B. B., "Greenhouse effect: greenhouse gases and their impact on global warming," 17, 6, 2018, 1-9. https://doi.org/10.9734/JSRR/2017/39630

[2] Herbert, G. J., Iniyan, S., Sreevalsan, E., and Rajapandian, S., "A review of wind energy technologies," 11, 6, 2007, 1117-1145. https://doi.org/10.1016/j.rser.2005.08.004

[3] Wang, S. and Wang, S., "Impacts of wind energy on environment: A review," 49, 2015, 437-443. https://doi.org/10.1016/j.rser.2015.04.137

[4] Kang, J. and Lee, H., "The development of rotor brakes for wind turbines," 12, 15, 2017, 5094-5100.

[5] Sirotkin, E., Solomin, E., Gandzha, S., and Kirpichnikova, I., "Backup mechanical brake system of the wind turbine," 944, 1, 2018, 012109. https://doi.org/10.1088/1742-6596/944/1/012109

[6] Hutchings, I. and Shipway, P., "Tribology: friction and wear of engineering materials," 2017, https://doi.org/10.1016/B978-0-08-100910-9.00003-9

[7] Ludema, K. C. and Ajayi, L., "Friction, wear, lubrication: a textbook in tribology," 2018, https://doi.org/10.1201/9780429444715

[8] Govindaraju, M., Megalingam, A., Murugasan, J., Vignesh, R. V., Kota, P. K., Ram, A. S., Lakshana, P., and Kumar, V. N., "Investigations on the tribological behavior of functionally gradient iron-based brake pad material," 234, 12, 2020, 2474-2486. https://doi.org/10.1177/0954406220905858

[9] Guha Keshav, M., Hemchandran, C. G., Dharsan, B., Pradhin, K., Vaira Vignesh, R., and Govindaraju, M., "Manufacturing of continuous fiber reinforced sintered brake pad and friction material," 46, 2019, 4493-4496. https://doi.org/10.1016/j.matpr.2020.09.686

[10] Rajesh Kannan, K., Govindaraju, M., and Vaira Vignesh, R., "Development of fly ash based friction material for wind turbines by liquid phase sintering technology," 235, 7, 2021, 1463-1469. https://doi.org/10.1177/1350650120963998

[11] Ahmed, K. A., Mohideen, S. R., Balaji, M., and Rajan, B. S., "Tribological Performance of Brass Powder with Different Copper and Zinc Content in the Brake pad," 42, 2, 2020, https://doi.org/10.24874/ti.783.10.19.03

[12] Baskar, S. and Sriram, G., "Tribological Behavior of Journal Bearing Material under Different Lubricants," 36, 2, 2014,

[13] Ilangovan, S., Vaira Vignesh, R., Padmanaban, R., and Gokulachandran, J., "Comparison of statistical and soft computing models for predicting hardness and wear rate of Cu-Ni-Sn alloy," 710, 2018, 559-571. https://doi.org/10.1007/978-981-10-7871-2_54

[14] Ilangovan, S., Vaira Vignesh, R., Padmanaban, R., and Gokulachandran, J., "Effect of composition and aging time on hardness and wear behavior of Cu-Ni-Sn spinodal alloy," 26, 10, 2019, 2634-2642. https://doi.org/10.1007/s11771-019-4200-x

[15] Kannan, K. R., Vignesh, R. V., Kalyan, K. P., Murugesan, J., Megalingam, A., Padmanaban, R., and Govindaraju, M., "Tribological performance of heavy-duty functionally gradient friction material (Cu-Sn-Fe-Cg-SiC-Al2O3) synthesized by PM route," 2128, 1, 2019, 020004. https://doi.org/10.1063/1.5117916

[16] Kumar, R. A., Sai, K. P., Vignesh, R. V., and Radhika, N., "Investigations on the Tribological Properties of Heat-Treated Copper Composite Using Hybrid Quadratic-Radial Basis Function Model," 72, 12, 2019, 3117-3128. https://doi.org/10.1007/s12666-019-01777-y

[17] Kannan, K. R., Vignesh, R. V., Kalyan, K. P., Murugesan, J., Megalingam, A., Padmanaban, R., and Govindaraju, M., "Tribological performance of heavy-duty functionally gradient friction material (Cu-Sn-Fe-Cg-SiC-Al2O3) synthesized by PM route," 2128, 2019, https://doi.org/10.1063/1.5117916

[18] Zhou, H., Yao, P., Xiao, Y., Fan, K., Zhang, Z., Gong, T., Zhao, L., Deng, M., Liu, C., and Ling, P., "Friction and wear maps of copper metal matrix composites with different iron volume content," 132, 2019, 199-210. https://doi.org/10.1016/j.triboint.2018.11.027

[19] Zhang, P., Zhang, L., Fu, K., Cao, J., Shijia, C., and Qu, X., "Effects of different forms of Fe powder additives on the simulated braking performance of Cu -based friction materials for high-speed railway trains," 414, 2018, 317-326. https://doi.org/10.1016/j.wear.2018.09.006

[20] Zhang, P., Zhang, L., Fu, K., Wu, P., Cao, J., Shijia, C., and Qu, X., "Fade behaviour of copper-based brake pad during cyclic emergency braking at high speed

and overload condition," 428, 2019, 10-23. https://doi.org/10.1016/j.wear.2019.01.126

[21] Gultekin, D., Uysal, M., Aslan, S., Alaf, M., Guler, M., and Akbulut, H., "The effects of applied load on the coefficient of friction in Cu-MMC brake pad/Al-SiCp MMC brake disc system," 270, 1-2, 2010, 73-82. https://doi.org/10.1016/j.wear.2010.09.001

[22] Abdi, S., Ouroua, Y., and Menchi, O., "Development and characterisation of metal matrix composite steel/Cu-Zn," 1, 1, 2009, 1-7. https://doi.org/10.3923/ajmskr.2009.1.7

[23] Zhang, P., Zhang, L., Fu, K., Wu, P., Cao, J., Shijia, C., and Qu, X., "The effect of Al2O3 fiber additive on braking performance of copper-based brake pads utilized in high-speed railway train," 135, 2019, 444-456. https://doi.org/10.1016/j.triboint.2019.03.034

[24] Kang, S., "A study of friction and wear characteristics of copper-and iron-based sintered materials," 162, 1993, 1123-1128. https://doi.org/10.1016/0043-1648(93)90131-5

[25] Hamada, A., Khosravifard, A., Kisko, A., Ahmed, E., and Porter, D., "High temperature deformation behavior of a stainless steel fiber-reinforced copper matrix composite," 669, 2016, 469-479. https://doi.org/10.1016/j.msea.2016.03.084

[26] Österle, W., Prietzel, C., Kloß, H., and Dmitriev, A., "On the role of copper in brake friction materials," 43, 12, 2010, 2317-2326. https://doi.org/10.1016/j.triboint.2010.08.005

Appendix

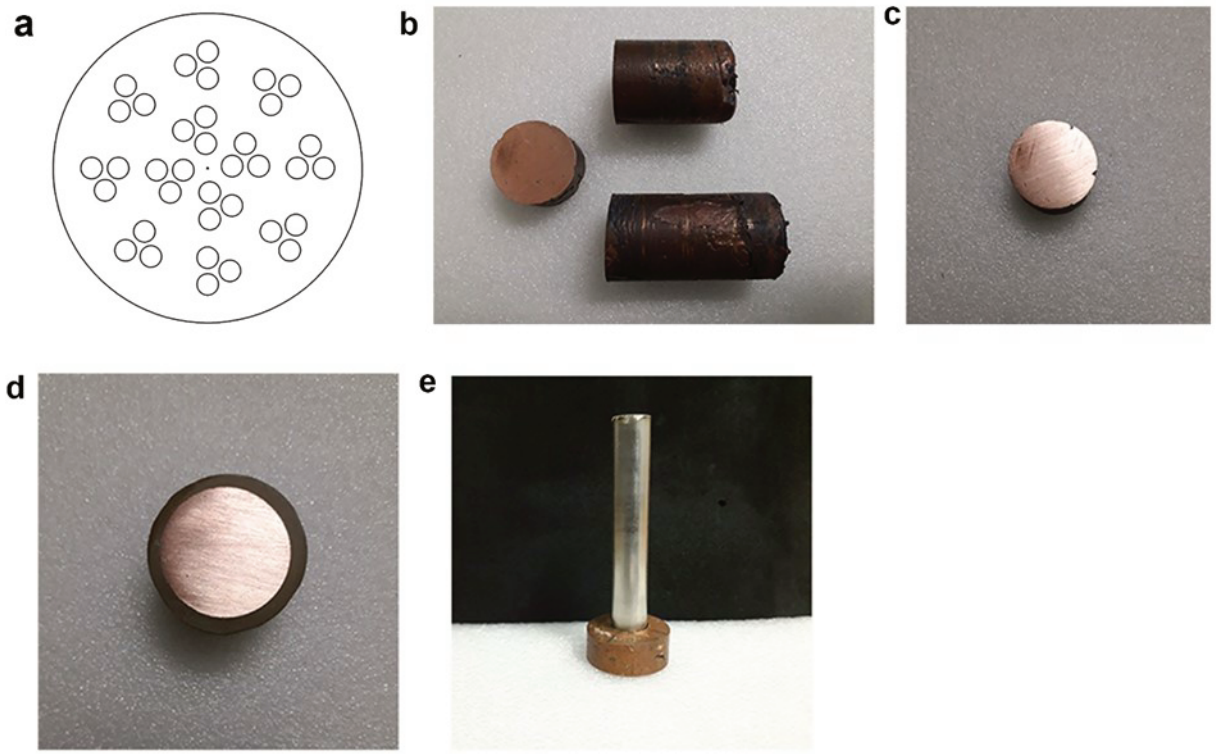

Figure. a) Representative image – plan of the composite specimen (small circles represent fibers' size not to scale); b) Fabricated specimen; c) Cut-section of the specimen; d) Specimen mounted for microstructural analysis; e) Specimen mounted for tribological analysis